Journal of Nuclear Materials 479 (2016) 436–446

Contents lists available at ScienceDirect

Journal of Nuclear Materials

journal homepage: www.elsevier.com/locate/jnucmat

Synthesis and characterization of Gd_2O_3 doped UO_2 nanoparticles

A.L. Soldati [a, b, *], I. Gana Watkins [a], A. Fernández Zuvich [a, c], F. Napolitano [a, b], H. Troiani [a, b], A. Caneiro [a, b, c], M. Prado [a, b, c]

[a] Centro Atómico Bariloche (CAB) – Comisión Nacional de Energía Atómica (CNEA), Av. Bustillo 9500, CP: 8400 Bariloche, Argentina
[b] Consejo Nacional de Investigaciones Científicas y Técnicas (CONICET), Av. De los Pioneros 2300, CP: 8400 Bariloche, Argentina
[c] Instituto Balseiro, Universidad Nacional de Cuyo, Av. Bustillo 9500, CP: 8400 Bariloche, Argentina

HIGHLIGHTS

- Synthesis of 4, 8, 10 and 15wt% Gd_2O_3 doped UO_2 nanoparticles.
- Crystallite sizes around 100 nm and rounded morphology.
- 90% Gd distribution homogeneity between particles for the less concentrated sample.
- High Statistic X-ray Rietveld analysis determined an $U_{1-x}Gd_xO_{2-\delta}$ fcc structure.
- Phases with similar crystal structure and symmetry, but different lattice parameter.

GRAPHICAL ABSTRACT

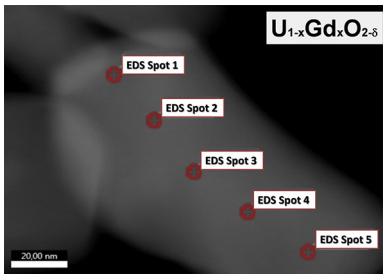

ARTICLE INFO

Article history:
Received 18 March 2016
Received in revised form
8 July 2016
Accepted 12 July 2016
Available online 15 July 2016

Keywords:
Burnable poison
Nuclear fuel
Nanoparticles
Microstructure
Chemical homogeneity
U–Gd solid solution

ABSTRACT

UO_2 nanoparticles doped with 4, 8, 10 and 15 wt% Gd_2O_3were synthesized by a reverse strike method. Crystal structure and chemical homogeneity were evaluated using a combination of X-ray diffraction and microscopy tools. An exhaustive study of the composition and its homogeneity at the micro and at the nanometer level was carried out in this nuclear fuel material. Field Emission Gun Scanning and Transmission Electron Microscopy images revealed the presence of micrometer scale agglomerates of nanoparticles, with rounded morphology and an average crystallite size of 100 nm. Rietveld refinements of high-statistic X-ray Diffraction data determined the crystal structure and composition. Furthermore, Energy Dispersive Spectroscopy using a 2 nm^2 spot on the sample surface determined a Gd concentration variation around the average of ±5% in different spots of a single crystallite and of ±10% between different crystallites. However, when measuring large amounts of nanoparticles the concentration averages, producing a homogeneous composition distribution at the micrometer scale.

1. Introduction

The study of actinide nanoparticles (NPs) has attracted the attention of the scientific community [10] not only because the lack of information about their ecotoxicological effects but also because their potential use for the nuclear energy production. On the one hand, biogeochemical effects of nano-particulated nuclear fuel materials is still controversial due to the enhanced reaction expected by the larger surface area of the particles, their increased mobility and their different redox chemistry when compared to micrometer scale material. Indeed, the chemical reactivity of actinides in the environment depends strongly on the particle

* Corresponding author. Centro Atómico Bariloche (CAB) – Comisión Nacional de Energía Atómica (CNEA), Av. Bustillo 9500, CP: 8400 Bariloche, Argentina.
E-mail address: asoldati@cab.cnea.gov.ar (A.L. Soldati).

http://dx.doi.org/10.1016/j.jnucmat.2016.07.033
0022-3115/

Abbreviations

NPs	Nanoparticles
HBS	High Burn up Structures
SEM	Scanning Electron Microscope
TEM	Transmission Electron Microscope
STEM	Scanning Transmission Electron Microscope
FEG	Field Emission Gun
EDS	Energy Dispersive Spectroscopy
XRD	X-ray Diffraction
ADU	Ammonium Diuranate

characteristics such as its grain size and biological availability, demanding the development of NPs for testing this topic. On the other hand, it was demonstrated that high burn up at low temperatures produces re-crystallization of UO_2 grains generating nanometer size particles at the periphery of the nuclear fuel, called High Burn-up Structures or HBS [11,19]. These HBS NPs exhibit closed porosity with better fission gas retention and radiation-tolerance, ameliorated mechanical properties, and less detriment of the thermal conductivity upon use [4,25], making them an interesting option for new nuclear fuels [18].

Recent efforts have been focused in finding different methods to produce and characterize actinide NPs, especially regarding the uranium species. The radiation chemical synthesis was one of the preferred methods to produce UO_2 NPs. This chemical route uses reducing (or oxidizing) agents, obtained by exposing the precursor solvents to ionizing radiation. Reducing agents force the reduction of U(VI) into U(IV) species, which coalesce to produce UO_2 particles with nanometer size. For example, ~80 nm and ~9 nm UO_2 NPs were synthesized from an uranyl-nitrate solution in presence of 2-propanol by using Co-60 γ and 6 MeV electrons irradiation, respectively [16]. Depleted UO_2, U-metal and U–lanthanide alloy NPs have been successfully synthesized from aqueous acidic salt solutions by γ radiation at temperatures as low as 500–600 °C [13,14]. The authors studied the reaction dependence of solution pH and reaction dose on the shapes, sizes, yield, and properties of the products. Other organic-phase synthesis method uses oleic acid, oleyl amine and 1-octadecene for producing size-controlled, nearly mono-dispersed, colloidal UO_2nano-crystals by thermal decomposition of uranyl acetyl acetonate [24,25]. In addition, ultrathin U_2O_3nanoribbons and U_3O_7 nano wires were produced from uranium acetate by a similar type of organic synthesis [9]. Further, oxalate precipitation was used to get nano-grained UO_2 powders with high crystallinity and particle sizes of about 10 nm [21]. Laser evaporation methods have been reported to produce UO_2 particles with tunable sizes and shapes [17]. Besides these chemical and radiolysis methods, uranium NPs were also produced by biological methods. For example, uraninite of around 3 nm was produced from uranyl acetate by *Shewanellaoneidensis* MR-1 cells [3].

Once a route has been selected for the actinide NPs synthesis, appropriate tools of the materials science are needed to fully characterize physical and chemical properties at the sub-micrometer scale level. Because of its excellent spatial resolution one of the best candidates for this kind of analyses is the Transmission Electron Microscopy (TEM) technique, where an electrons beam with energies around hundreds of keV passes through a thin sample (<100 nm), interacting with the material and providing a set of complementary information. In addition, by focusing the electron beam with a Field Emission Gun (FEG), the TEM can be used in scanning mode (STEM) and has high enough current to perform elemental analyses even at an atomic scale resolution [26]. Thus, many characteristics of the NPs, such as morphology, grain size, signs of stress and degradation, crystal defects induced by synthesis, thermal treatment or radiation damage, among other parameters can be found through transmission images in Bright Field (BF), Dark Field (DF) or High Resolution (HR) modes [22]. Moreover, the analysis of Selected Area Electron Diffraction (SAED) patterns allow identification of crystal phases, signs of degradation or amorphization and presence of precipitates and, when coupled to an Energy Dispersive Spectroscopy (EDS) detector, the transmission microscope provides local information about the chemical composition even in volumes of only some nanometers in size.

In this work, we investigated Gd-doped U nanoparticles. Thanks to its large neutron absorption cross-section and the fact that its activation product does not absorb neutrons, Gd is used as a burnable poison that helps to control the reactivity at the beginning and at the end of fuel cycle [2,8]. We synthesized 4, 8, 10 and 15 wt% Gd_2O_3 doped UO_2 NPs by the well known "Reverse Strike" co-precipitation method [6,15]. We used a FEG-SEM, a FEG-TEM/STEM and a TEM equipped with a LaB_6 filament, all of them coupled with EDS analysers and capable of determine the composition, microstructure and morphology of the sample, down to the nanometer level. In addition, we determined the crystalline phases present in the bulk as well as in single nano-crystallites by using both, Electron and X-ray diffraction. Thus, this work resulted in a detailed analysis of crystal structure and composition homogeneity at the nanometer scale in four U–Gd solid solutions, supplying with a set of well characterized NPs, which will be the raw material for future research in nuclear fuel development, eco-toxicology and environmental impact assessments.

2. Materials and methods

2.1. Material synthesis

UO_2 doped with 4, 8, 10 and 15 wt% Gd_2O_3 were prepared by the "Reverse Strike" co-precipitation method [6,15]. This is a wet chemical route were Uranium and Gadolinium oxides are dissolved in 65% HNO_3 under continuous stirring and react drop by drop with NH_4OH at constant temperature (60 °C) and pH (9) in an aqueous solution. As a result, a mixture of Ammonium Diuranate (ADU) and $Gd(OH)_3$ is obtained. The product suspension (approximately a volume of two liters) was then filtered, washed several times with milliQ water and let dry overnight at 100 °C. Subsequently, the material was calcined at 800 °C in air for 4 h. The obtained product (around 100 g) was reduced in Noxal atmosphere (5 vol % H_2:Ar) at 650 °C to obtain an $(U,Gd)O_2$ solid solution.

From these reduced precipitates two batches of samples were prepared (Table 1):

2.1.1. Batch N (N4, N8, N10 and N15)

The as reduced powders were manually crashed and milled with an agate mortar for some minutes, with no further treatment. Samples N have nanometer scale grain sizes and are the target of this study.

2.1.2. Batch S (S4, S8, S10 and S15)

In these case, samples provided by Batch N were compacted with an uni-axial press (50 kN for 30 s) and further sintered at 1700 °C in Noxal atmosphere for 2 h, resulting in samples with micrometer scale grains size which allows the comparison with already published data.

Table 1
Nano and micrometer scale samples studied in this work. (a) Composition obtained by averaging three SEM-EDS measurements in a 20 × 20 μm window (average ± standard deviation, using U_M and Gd_L lines for quantification (semi-quantitative); SEM operation V = 20 keV). (b) Composition obtained by averaging five TEM-EDS measurements in a 200 × 200 nm window (average ± standard deviation, using U_L and Gd_L lines for quantification (semi-quantitative); TEM operation V = 200 keV).Temperatures used for oxidation in air (Ox), and reduction (Red) and Sintering (Sint) in 5 vol % H_2:Ar.

Nominal composition			Name	Measured concentration Gd [at%][b]		Temperature [°C]		
Gd_2O_3 [wt%][a]	Gd [at%][b]	$U_{1-x}Gd_xO_{2-\delta}$		SEM-EDS(a)	TEM-EDS(b)	Ox	Red	Sint
4.0	5.8	$U_{0.94}Gd_{0.06}O_{2-\delta}$	N4	6.9 ± 0.7	8 ± 2	800	650	–
			S4	7.0 ± 0.3	5 ± 2	800	650	1700
8.0	11.5	$U_{0.89}Gd_{0.11}O_{2-\delta}$	N8	14 ± 1	14 ± 1	800	650	–
			S8	12.5 ± 0.5	11 ± 1	800	650	1700
10.0	14.2	$U_{0.86}Gd_{0.14}O_{2-\delta}$	N10	16.2 ± 0.5	16 ± 1	800	650	–
			S10	16.0 ± 0.5	15.6 ± 0.4	800	650	1700
15.0	20.8	$U_{0.79}Gd_{0.21}O_{2-\delta}$	N15	21.7 ± 0.2	23.7 ± 0.8	800	650	–
			S15	22.6 ± 0.1	23.5 ± 0.9	800	650	1700

[a] The nominal contents for Gd_2O_3 [wt%] are conventionally reported as weight percentage of the oxide (Gd_2O_3) to the sum of UO_2 and Gd_2O_3.
[b] The nominal contents for Gd [at%] are conventionally reported as atomic percentage of Gd to the sum of U and Gd atoms.

2.2. Transmission Electron Microscopy (TEM)

Samples N were prepared for TEM analysis. For that, a homogeneous suspension of some milligrams of powdered material in 1 ml isopropyl alcohol was prepared by ultrasonication during 5 min. A drop of the obtained suspension was transferred to a gold TEM grid (ultra-thin carbon film type A, 300M, Ted Pella®) and then allowed to dry in air. Two transmission microscopes were used for the analysis: A Philips CM200 Ultra Twin with LaB_6 filament and a FEI TECNAI F20 FEG-TEM/STEM operated at 200 keV. Both microscopes are coupled to EDS systems for elemental quantification: the first one is equipped with a EDAX-Genesis Si(Li) detector and the second one with a EDAX-Apolo Silicon Drift Detector (SDD). TEM images were acquired using CCD cameras and the commercial softwares Digital Micrograph© and Item©. The crystallite sizes were characterized by their longest dimension (i.e. the diameter in case of a quasi spherical morphology). The crystallites size distribution was fitted with a Log Normal function and the characteristic size was calculated as the arithmetic average ± (standard deviation/$\sqrt{n}$), where n is the number of measured crystallites.

Sample N4 was scanned in the nano-probe mode by combining the High-Angle Angular Dark Field (HAADF) and the EDS detectors. For that, a convergent electron beam of 2 nm^2 (on the sample surface) was used. The EDS spectra were integrated during 200 s, on the 0–20 keV energy range, with a counting rate of at least 500 cps and a dead time of less than 20%. Posterior data and images treatments were done both with the commercial programs TEAM© and Digital Micrograph©, respectively. Only the Lα X-ray emissions were used for quantification (GdL_α = 6.05 keV and UL_α = 13.615 keV, respectively). Using these conditions, the less concentrated sample signal to noise ratio is 3 for GdL_α and 50 for UL_α. Indeed, the detection limit for Gd in this matrix and with this experimental setup could be considered at half of the measured concentration (i.e. 2.0 wt%; details of a typical spectrum are given in Fig. 6C). Nevertheless, the quantification performed here should be considered semi-quantitative, because no standards were measured for direct calculation. The local composition (Gd/(U + Gd) at%) was calculated for each crystallite as the mathematical average obtained in five different points of each single crystallite. Then, the composition variation between different crystallites was compared to find the homogeneity at a nanometer level in the less concentrated (4 wt%) Gd_2O_3 doped UO_2 matrix.

2.3. Scanning electron microscopy (SEM)

Nanoparticles morphology and agglomeration in samples N were studied with a Nova Nano SEM 230 equipment, operated between 2 and 20 keV with a Schottky FEG and equipped with a SDD Genesis EDAX-EDS spectrometer for semi-quantitative composition analyses and elementary mapping. For the FEG-SEM analyses the powder was directly mounted on a conductive tape and gold sputtered. The FEG-SEM-EDS element mappings were performed on the surface of a pressed pellet that was previously sputtered with Gold to avoid charge accumulation. The images were obtained at a magnification of 25000X with a resolution of 256 × 350 pixel and a dwell time of 1000 ms. U_M and the Gd_L X-ray emission lines were used for the compositional analysis.

2.4. X-ray diffraction (XRD)

Diffraction patterns of the powdered samples were measured at room temperature in a PANalytical Empyrean® device with C monochromator (CuK_α) and a PixCel3D detector, using a Bragg-Brentano configuration. Scans were measured in the 20°–130° 2θ range with a step of 0.02° and an acquisition time of 150 s/step. The present phases were identified with the program Xpert® and the average crystallite size was determined using the Scherrer equation. High statistic XRD patterns were collected and analyzed by the Rietveld method using the Fullprof Suite software [5].

The structural models used as input in the Rietveld refinements were based on the well-known UO_2 structure [23]. This choice was based on the similarity between the XRD patterns of UO_2 and Gd-doped UO_2 indicating that structure symmetry should be the same (Fm-3m space group), and the assumption that Gd is incorporated into the structure in the same crystallographic site than U (Wyckoff position 4a), but randomly distributed. Peak profiles were fitted using Thompson-Cox-Hasting functions [20] with axial divergence in order to directly include micro-strain and size effects as refinable parameters. Additionally, the site-specific isotropic atomic displacement parameters were also incorporated into the refining process.

A stability test of the NPs was performed in order to evaluate possible phase degradation or re-oxidation after the thermal treatment at 700 °C in 10 vol% H_2:He atmosphere. For that, sample N8 was placed into an Anton Paar HTK1200 high temperature chamber with a continuous flux of 10 vol% H_2:He, and measured in-situ as temperature followed 25°C–700 °C – 25 °C cycle (10 °C/min, 8 h of dwell time).

3. Results

3.1. Morphology and crystal size of the (U,Gd)O_2 nanoparticles

TEM images show that all N samples (Fig. 1) correspond to

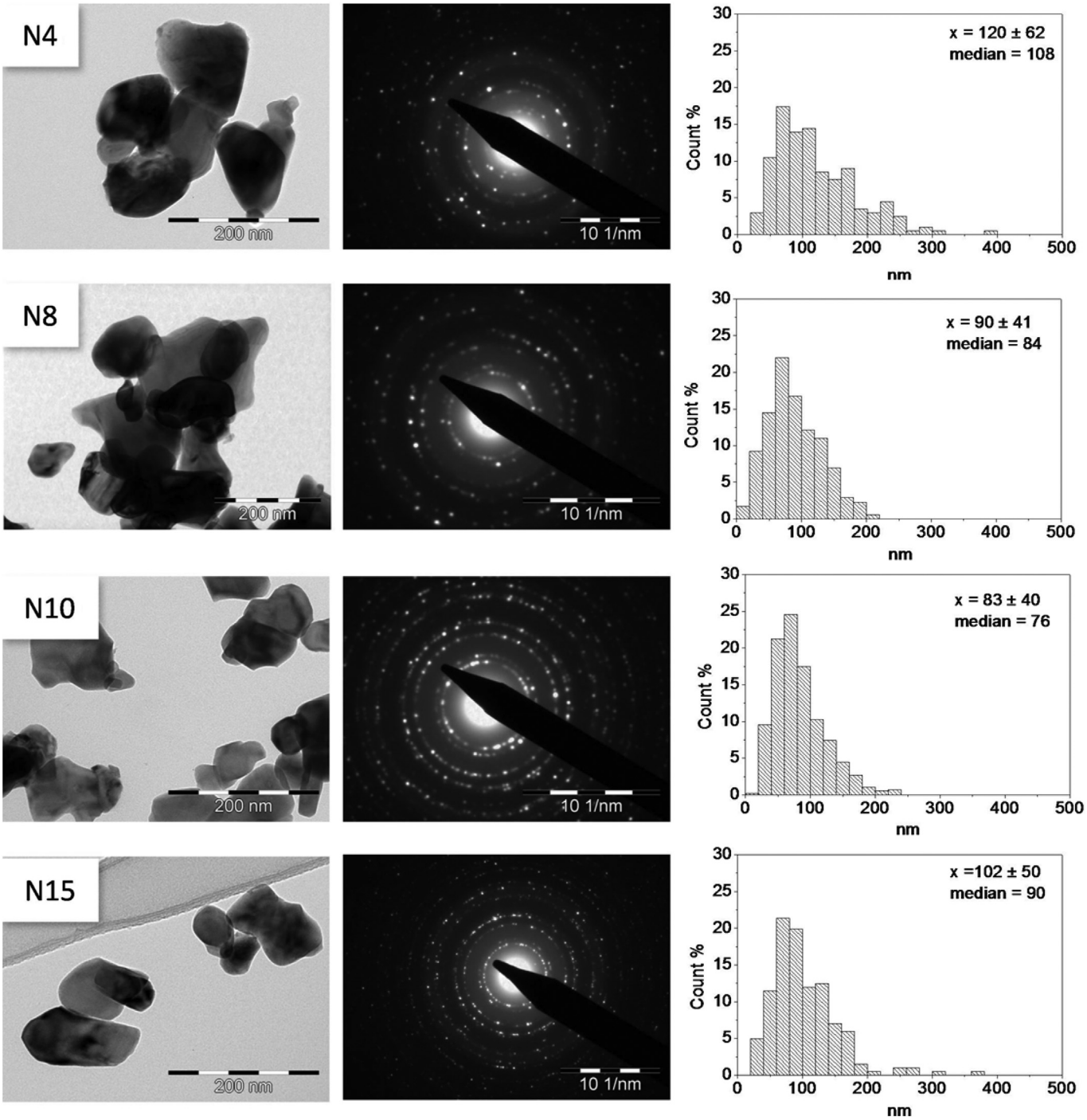

Fig. 1. TEM images of N samples (left) showing the typical diffraction pattern (centre) and the crystallite size histogram (right). The average crystallite sizes remain around 100 nm.

particles with crystallite sizes in the nanometer range (<300 nm), while S samples have crystallites that are larger than one micron (Fig. 2). A characteristic length (*Lc*) histogram (Fig. 1, right column) was reconstructed from the data measured in different TEM and STEM images of the NPs. Using a Log Normal distribution for the statistical analysis, it was verified that the crystallite size in the Gd_2O_3 doped UO_2 materials results around 100 nm. Furthermore, the comparison of the histograms shows that the N8 and N10 samples possess smaller crystallite sizes with narrower distributions than the two extreme samples (N4 and N15) of the series studied here.

TEM images acquired in scanning mode show that the Gd_2O_3 doped UO_2 nanoparticles, synthesized by the reverse strike method, agglomerate forming micrometer scale aggregates (Fig. 3A). The single crystallites (Fig. 3B) are recognized by their homogeneous gray tone and defined outline. Besides, SAED of the agglomerates show concentric circles (Fig. 3C), supporting the poly-crystalline nature of the sample. The diffraction patterns can be

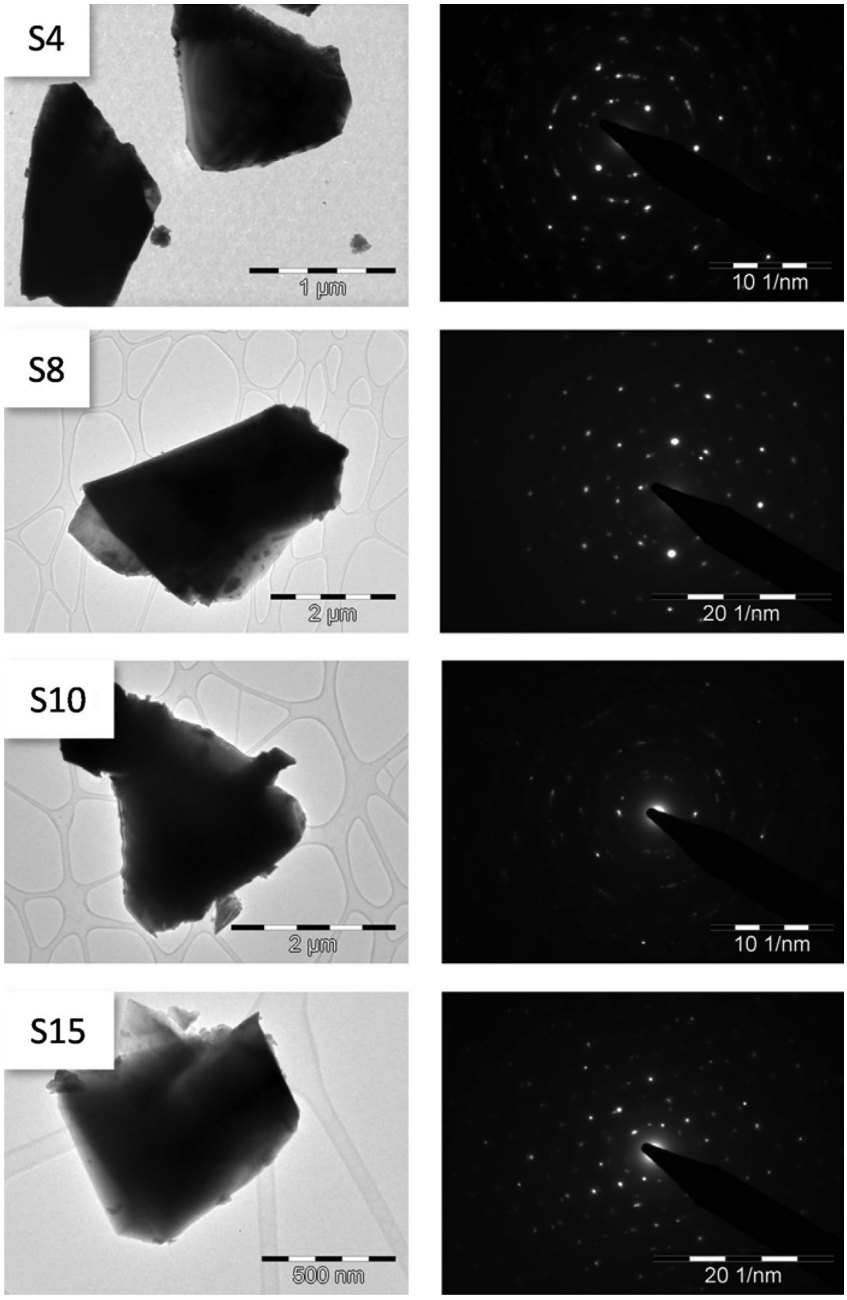

Fig. 2. TEM images of S samples (left) showing the typical diffraction pattern (right). Average crystallite sizes are larger than 1 μm.

indexed correctly with the cubic structure of UO_2. In addition, the SAED of a single crystallite (Fig. 3D) shows a mono-crystal pattern corresponding to a fluorite structure (axis zone: $2\bar{4}\bar{2}$). This indicates that each of the observed crystallites within an agglomerate are single-crystal domains.

TEM bright/dark field contrast (Fig. 4) is also useful to identify the single crystallites in an agglomerate. Single crystallites are clearly observed as white particles in DF-TEM images (Fig. 4A) and as black/gray particles in the BF-TEM mode (Fig. 4B). Furthermore, HR-TEM images (Fig. 4C and D) allow us to determine predominant atomic directions in each particle. The particles that form the agglomerates are all well crystallized single domains, because each one has a unique atomic orientation. In addition, the atomic planes are very well defined up to the particle border and no amorphous zones can be detected at the crystallites boundaries or inside them. The smallest crystallites observed are between 10 and 30 nm, while only few particles reach more than 200 nm.

3.2. Chemical composition of the $(U,Gd)O_2$ nanoparticles

Fig. 5 shows an example of the FEG-SEM secondary electrons micrographs obtained from the lowest doped sample (N4). Similar results were observed for all other compositions. In agreement with TEM images, agglomerates of crystallites with rounded forms can be observed at low magnifications (Fig. 5A). Higher magnifications (Fig. 5B) allow detection of sub-micrometer scale structures. A backscattered electrons micrograph of the powder sample is shown in Fig. 5C. Despite the appreciable difference between the U and the

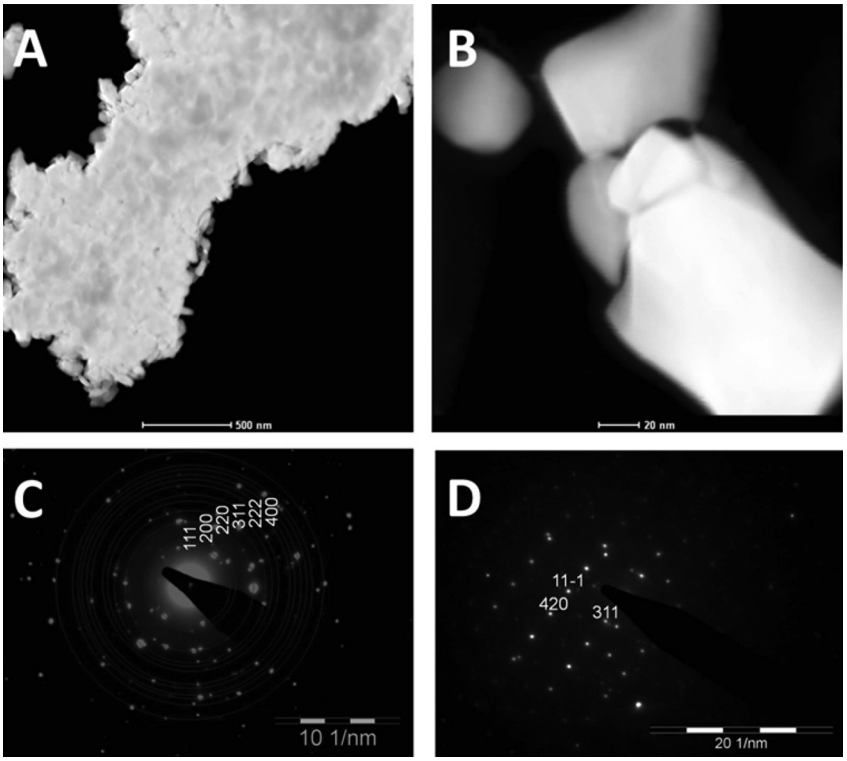

Fig. 3. STEM images of sample N4 showing an agglomerate (A) and a group of nanoparticles (B). SAED of an agglomerate (C) and of a single crystallite (D). The diffraction patterns show a fluorite structure. The same indexation was obtained for the other N samples (see Fig. 1).

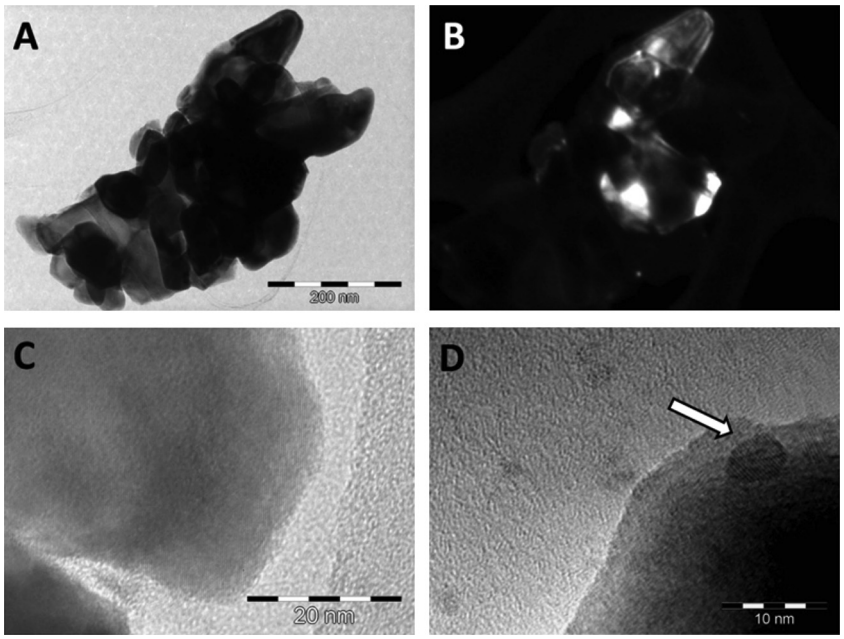

Fig. 4. BF-(A) and DF-TEM (B) images of N4 nanoparticles obtained using the objective aperture N°3. HR-TEM images showing the atomic planes in different crystallites (C and D). The arrow in D shows a <10 nm crystallite.

Gd atomic masses, no clear Z contrast can be observed in this image, suggesting a solid solution with homogeneous composition at this scale. Fig. 5D shows the surface of a (U,Gd)O_2 pellet. The nanocrystallites can be distinguished at the magnification used there. However, EDS maps of the elements U (Fig. 5E) and Gd (Fig. 5F) achieved at the same magnification do not detect any heterogeneity in the composition. This could be a result of both, a real homogeneous distribution of the Gd in the UO_2 matrix or a composition averaging due to the resolution of the FEG-SEM-EDS instrument and the nanometer scale of the particles. In order to solve this issue, a technique with better spatial resolution is needed and therefore discussed in the following section.

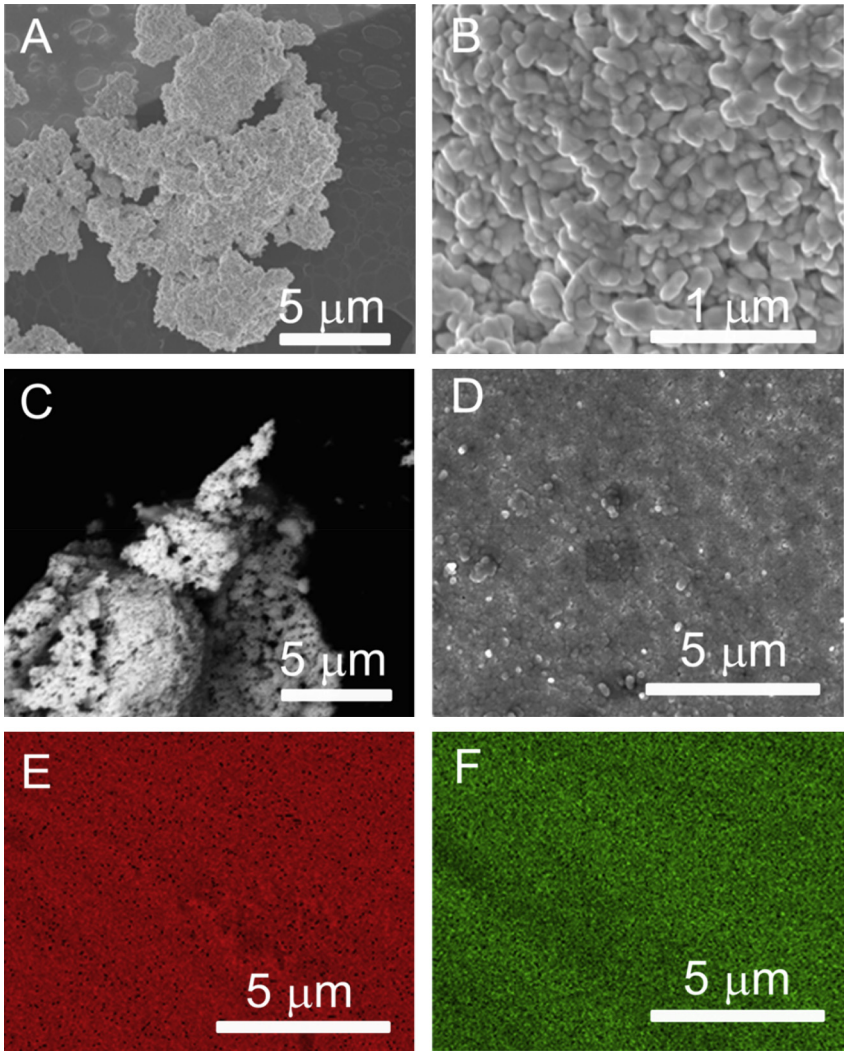

Fig. 5. Micrographs obtained by FEG-SEM and elemental maps obtained by FEG-SEM-EDS for the sample N4. Image of secondary electrons (5 keV) of the (U,Gd)O_2 nanoparticles, obtained using the TLD lens to reach higher magnifications (A–B). Image of backscattered electrons (15 keV) at the highest possible magnification with this microscope, performed with the GAD detector; no differences in composition can be detected with this technique (C). Surface of a (U,Gd)O_2 pellet, performed with secondary electrons (20 keV) using the ETD detector (D). EDS map of composition showing the elements Uranium (E) and Gadolinium (F); these maps were performed using 20 keV electrons for excitation.

3.3. *Sample homogeneity at the nanometer level*

With the aim of evaluating the homogeneity of the NPs, down to the nanometre level, the composition in one of the samples was analyzed by FEG-STEM-EDS. In this case, sample N4 with an expected nominal composition of (Gd/(U + Gd) = 5.8 at%) was selected for the analysis because it is the less concentrated sample, and allows to identify the detection limits of the techniques applied here. A total of 14 crystallites were analyzed. At each crystallite, 5 EDS spectra were obtained at different points, and a mean value for each element was calculated. The points were preferably selected well distributed over the crystallite (Fig. 6A). Thus, each point shown in Fig. 6B represents the average composition of a single crystalline domain. Typical spectra obtained are shown in Fig. 6C.

The analyses showed the presence of U and Gd in all points of all measured nano-crystallites. This result was expected after using the reverse strike method for the synthesis because the precursor oxides are dissolved in nitric acid, forming a homogeneous solution. However, the FEG-STEM-EDS experiment revealed variations in the Gd distribution at the nanometer level that are compensated at the microscopic level by averaging a large number of NPs. Indeed, the absolute mean concentration value resulted in (8.2 ± 1.7) at% (Fig. 6B), which is larger than the expected nominal composition (5.8 at%) but is consistent with the mean composition found by TEM-EDS averaging five windows of 200 × 200 nm^2 (8 ± 2) at% and is within the uncertainty interval of the composition measured by FEG-SEM-EDS (6.9 ± 0.7) at% averaging 200 × 200 μm^2 areas (Table 1). Moreover, the mean standard deviation (SD) found inside the nano-crystallites was ±15%. In comparison, the composition dispersion found between the different crystallites was ±20%. It is worth to note here that 10% of the standard deviation corresponds to instrumental and measurement uncertainties (SD_i).[1] The other part of the variance (i.e. (SD-SD_i) = 5% for single crystallites and 10% between different crystallites) should be related to the intrinsic composition heterogeneities of the samples at the nanometre scale. This value can be used as indicator to characterize the Gd composition heterogeneity or best, its complement, the homogeneity

[1] The instrumental uncertainty was calculated measuring 5 times the same point in one nano-crystallite. This value is related to the TEM-EDS equipment and to the Gd detection limit at the concentration analyzed here.

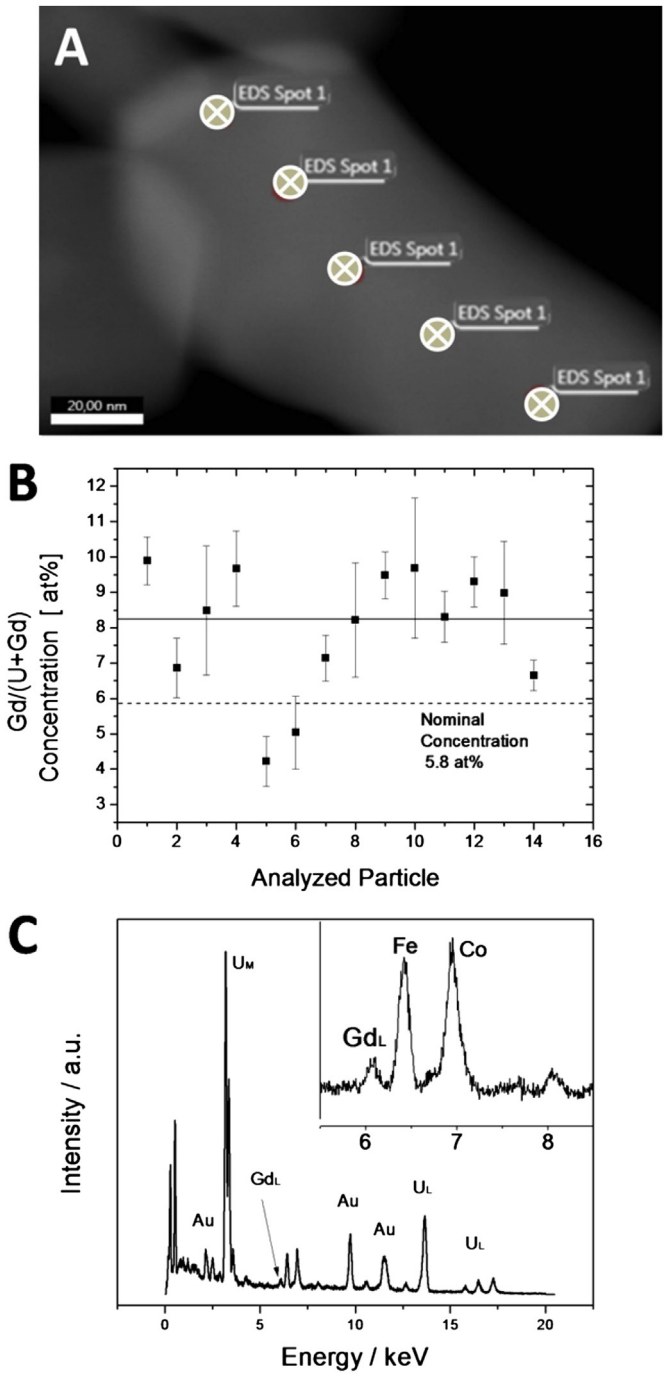

Fig. 6. Example of a FEG-STEM-EDS analysis in a nano-crystallite of sample N4, showing the specific points where the EDS probes were performed. Each area analyzed is around 2 nm^2(A). Gd concentration measured as Gd/(U + Gd) at% at different nano-crystallites(B). The error bar in each point shows the standard deviation of 5 measurements in different places of a single crystallite. Typical EDS spectrum (C): Au signal is originated from the TEM grid and Co and Fe are interference signals of the microscope, and are independent of the sample. The inset shows the Gd_L peak used for semi-quantification.

around the average concentration.

3.4. Crystalline phases

XRD measurements at different steps of the NPs synthesis showed the transition from the precursors UO_2 and Gd_2O_3 (Fig. 7)

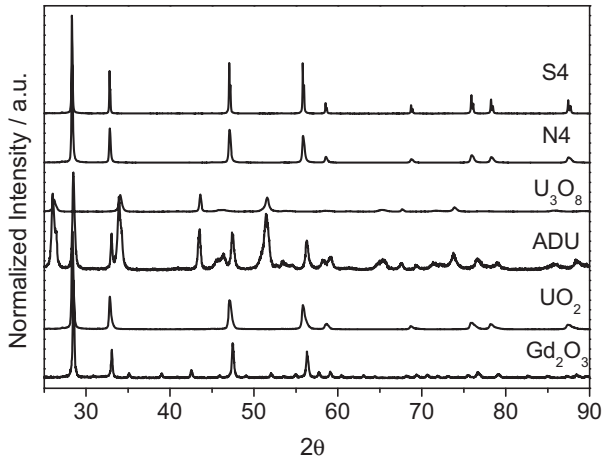

Fig. 7. X-ray diffractograms showing the oxide precursors used for the synthesis (natural UO_2 and Gd_2O_3), the intermediate phases (ADU and U_3O_8) and the final (U,Gd)O_2 materials (N4: nanometer scale and S4:micrometer scale) for the sample doped with 4 wt % of $Gd_2O_3/(UO_2+Gd_2O_3)$.

to the final N and S compounds, passing through intermediate states with characteristic peaks associated to ADU and U_3O_8. The final product can be identified with a unique crystalline phase with cubic Fm-3m structure and cell parameters slightly shifted from the UO_2 reference sample (Powder Diffraction Card N 01-075-0420, International Centre for Diffraction Data, Newtown Square, PA). In addition, the presence of Gd_2O_3, as a segregated phase, was not detected in the final product.

The lattice parameters and the crystal structure of the UO_2 precursor and of samples N and S, were calculated by Rietveld analysis with the Fullprof Suite software, and are shown in Figs. 8 and 9, and in Table 2.

The sintered samples present a linear decrease of the lattice parameter with increasing Gd concentration (Fig. 9), as was expected by the Vegard's law. The XRD diffractogram can be completely reproduced by modeling an $U_{1-x}Gd_xO_{2.00}$ system with the nominal composition, and a unique phase with fcc structure and Fm-3m space group. In this structure the Gd^{3+} atoms are replacing the U^{4+} atoms in the same crystallographic site.

In opposition, the NPs XRD diffractograms cannot be modeled with a single phase. This is clearly observed, for example, by comparison of the residues between the measured and the calculated curves (Fig. 8B) considering only one homogeneous phase (right) or two phases (left). In the cases of N4, N8 and N10 two phases were necessary to fit the diffractograms successfully, while three phases were needed to reduce the chi square function of the N15 fit (Fig. 8 and Table 2). The additional phases have the same structure, crystallographic positions and symmetries, but they differ in the lattice parameter values.

For N4 and N10, one of the phases has the same lattice parameter than the partner S samples (called “phase 2”) and the other phase possess lower values. For N8 the two phases have a different lattice parameter: in one case is higher and in the other case is lower than the sintered S8. In the case of N15 one phase has a lattice parameter that coincides with the sintered partner S15 (“phase 2”), one possess a higher value and other a lower one.

From the lattice parameters of each individual phase, a characteristic Gd concentration (called “individual concentration” in Table 2) was determined by using the linear regression published by Baena, Cardinaels et al. [1]. Then, an “average” Gd concentration was determined for each sample taking into account the proportion of each individual phase and its corresponding individual

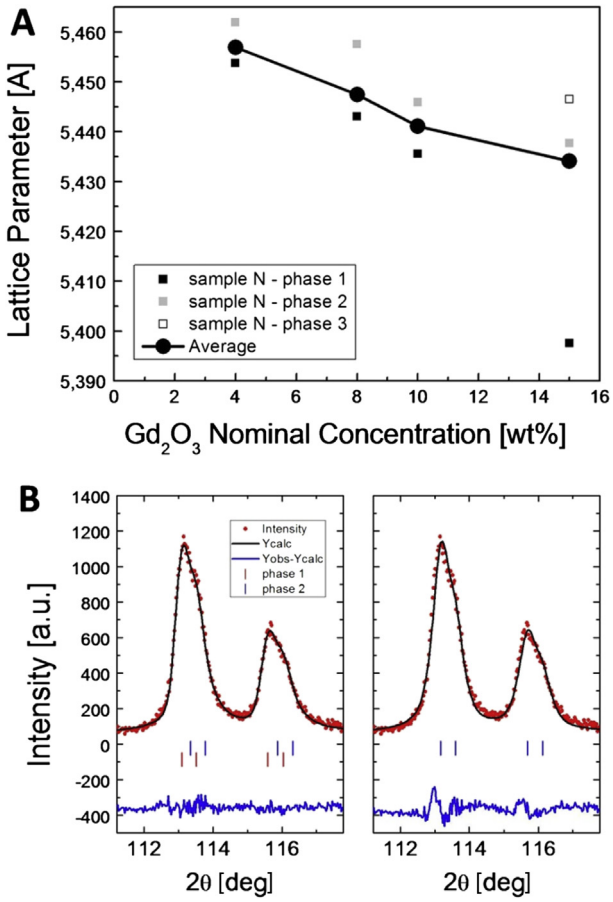

Fig. 8. (A) Lattice parameters obtained from XRD Rietveld refinements for the different phases found in the nanometer sized samples. The average was calculated taking into account the phase proportions indicated in Table 2. (B) Rietveld refinement of sample N4 using for the calculation two phases (left) or one single phase (right), showing that this latter is not sufficient to fit the diffractogram adequately (observe the residues between the experimental and the calculated intensity).

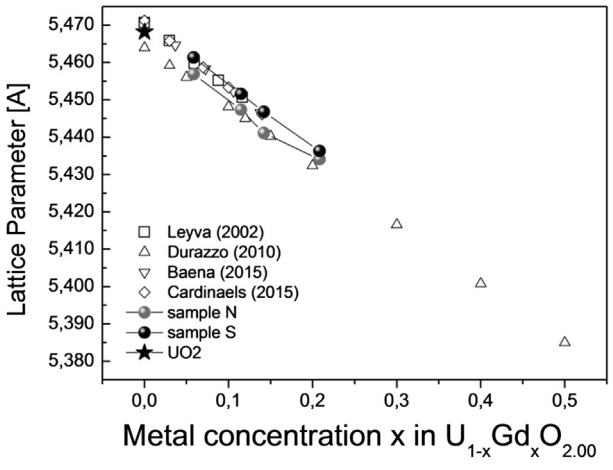

Fig. 9. Average lattice parameters obtained from XRD data for the precursor UO_2, the nano-particulated (N) and the sintered (S) samples. Data of sintered samples extracted from literature are plotted in open symbols for comparison. Error bars are smaller than the point used.

concentration. In the same way, individual and average lattice parameters were calculated for each phase or sample respectively, and are shown in Fig. 9 (and Table 2), together with the lattice parameters obtained for the sintered batch of samples and for data reported in the literature.

A lattice contraction parameter can be calculated for both $U_{1-x}Gd_xO_{2.00}$ systems, by linear regression of each batch of samples. On one hand, the sintered samples have a lattice contraction parameter of −16.7 ($R^2 = 0.999$), which follows the Vegard's law and is in agreement with previously reported data on $(U,Gd)O_2$ synthesized by the reverse coprecipitation method (See Ref. [1] and references cited there). On the other hand, the nanometer sized samples have a lattice parameter contraction that, as expected from the Rietveld results, is lower and more dispersed than that measured for the sintered partners showing a lattice parameter contraction of −15.6 ($R^2 = 0.918$). NPs data, however, are very close to the data presented in the work of [6].

4. Discussion

The lattice parameter contraction in the UO_2-Gd_2O_3 solid solution system was already studied by many authors [1,6,7,12]. These studies were carried on in samples obtained by mechanical milling and/or using a co-precipitation method similar to the one used here; but, in all those works the samples were sintered around 1700 °C in a reducing atmosphere yielding micrometer scale size particles. For those cases, the presence of $U_{1-x}Gd_xO_2$ with a unique fcc fluorite-phase (and the absence of peaks corresponding to Gd_2O_3 phases) were reported for x in the range $0 < x < 0.5$. Furthermore, the authors observed a linear lattice parameter contraction with the increase of Gd concentration and proposed that the Gd^{3+} ions are replacing the U^{4+} atoms in the UO_2 fluorite structure, due to the conversion of U^{4+} to U^{5+} and U^{6+} to compensate charge. The Rietveld analyses support this scenario for the samples sintered at 1700 °C in this work, but not exactly for the NP material.

A possible explanation to this is that a post-synthesis oxidation process may have occurred in the NPs. Such processes are commonly favored by the NPs higher surface area and the fact that these samples were stored in air during some months. To test this hypothesis, an XRD in situ experiment was performed with the high-temperature Anton Paar chamber. Sample N8 was further treated in a reducing atmosphere (10 vol% H_2:He) at 700 °C for eight hours, with a 10 °C/min heating/cooling ramp. The diffractograms acquired at 0, 3 and 7 h of treatment, and after the cooling, were refined with the Rietveld method and compared. No changes were observed (data not shown), indicating that the samples were not oxidized with the time.

Another hypothesis that could explain the difference between both batches is that the NPs may have slightly differences in composition, oxygen stoichiometry or speciation of the Uranium atom (U^{4+}, U^{5+} or U^{6+}), which homogenize after the sintering treatment at higher temperatures in a reducing atmosphere. The hypothesis that different particles may have different Gd concentrations was already observed in other cases. For example, fractionation of Gd in rich/depleted doped UO_2 oxides was reported in micrometer scale size particles obtained by inhomogeneous mechanical milling, for a Gd/(Gd + U) concentration ratio of 8 wt% [12]. In addition, the TEM, STEM and SEM coupled EDS analyses performed in this work also support slight differences in composition, even inside one NP. Regrettably, the quality of the present laboratory XRD data is insufficient to make better approximations with the Rietveld method, that would allow to identify different oxidation states of Uranium or oxygen hyperstochiometry. Synchrotron experiments would be necessary to undoubtedly resolve the structure in the nanometer scale samples, but are out of the scope of the present work.

Table 2
Lattice parameters and goodness-of-fit parameters obtained from the Rietveld refinements of $U_{1-x}Gd_xO_{2-\delta}$ series. (I) Average lattice parameters were calculated as the mathematical average of each individual lattice parameter weighted by the proportion of the corresponding phase. (II) The Gd concentrations of each phase was calculated from the individual lattice parameters using the curve presented by Baena, Cardinaels et al. [1]. (III) The average Gd concentration for each sample was calculated as the mathematical average of each individual concentration weighted by the proportion of the corresponding phase. (IV) Crystallite sizes were calculated from the Scherrer equation on the (200) reflection for the nanometer scale samples.

Name	Rietveld phase		Lattice parameter [Å]		Gd conc.[II] [%at]		Cryst. size [IV]	Goodness of fit parameters		
	#	[%]	Individual	Average[I]	Individual	Average[III]	[nm]	Rwp	Re	χ^2
N4	1	61	5.45373(2)	5.4569(1)	9.8 (1)	8.03(8)	140	11.8	7.81	2.292
	2	39	5.46186(2)		5.3(1)					
S4	1	100	5.46135(5)	5.46135(5)	5.54(3)	5.54(3)	-	12.2	8.02	2.300
N8	1	70	5.44301(2)	5.4473(2)	15.8(1)	13.35(9)	81	10.5	8.20	1.635
	2	30	5.45756(2)		7.7(1)					
S8	1	100	5.45161(5)	5.45161(5)	10.98(3)	10.98(3)	-	11.9	7.64	2.430
N10	1	46	5.43553(2)	5.4411(1)	20.0(1)	16.86(8)	72	10.4	7.88	1.738
	2	54	5.44584(2)		14.2(1)					
S10	1	100	5.44681(5)	5.44681(5)	13.66(3)	13.66(3)	-	11.5	7.49	2.348
N15	1	15	5.39752(2)	5.4341(1)	41.2(1)	20.76(7)	74	10.5	8.09	1.678
	2	57	5.43765(2)		18.8(1)					
	3	28	5.44649(2)		13.8(1)					
S15	1	100	5.43631(5)	5.43631(5)	19.53(3)	19.53(3)	-	12.4	7.67	2.598

Regarding the composition of the samples, the lattice parameter obtained from XRD Rietveld refinements can be used to calculate the metal fraction in the solid solutions. The concentrations obtained in this way (Table 2) resulted in agreement with the EDS analyses performed by SEM and TEM/STEM (Table 1 and Fig. 6), inside the uncertainty interval of those measurements, validating all three experimental procedures.

5. Conclusions

This work demonstrated that the reverse strike method is a useful synthesis route to obtain $(U,Gd)O_2$ NPs for scientific and technological uses. SEM, TEM and STEM imaging showed that the material obtained is composed of agglomerated nano-crystallites with rounded morphology and characteristic lengths around 100 nm. X-ray and Selected Area Electron diffraction coincided with a fcc structure (Fm-3m), where Gd atoms are replacing the U atoms in the fluorite structure. In addition, Rietveld refinements of X-ray diffraction patterns helped to identify different phases that could be easily overlooked otherwise due to their similarities in crystallographic symmetry and structure. Besides, FEG-STEM-EDS analyses showed that the Gd concentrations distributes around the average in an interval of ±10% between nano-particles and of ±5% in single crystallites for the less concentrated samples (4 wt%). However, FEG-SEM-EDS studies on this material demonstrated that this difference in the Gd distribution at the nanometer scale averages when probing a large number of nanoparticles. Thus, these NPs have a homogeneous composition at the micrometer scale. Ongoing studies will help to evaluate the implications of the obtained grain size, morphology, chemical and structural variability in the thermal properties, porosity, plasticity, radiation damage, long-term stability, fission gas retention, eco-toxicity, etc. This information will help to determine whether these NPs are advantageous as nuclear fuels, from the performance as well as from the environmental point of view.

Acknowledgements

The authors thank for the financing support to ANPCyT (PICT 2013–0262 and PICT 2013-1403). Adriano Geracci Paula Troyon; Manuel Corte and Daniel Wilberger are gratefully acknowledged for the technical support with the TEM, SEM and the XRD equipments.

References

[1] A. Baena, T. Cardinaels, K. Govers, J. Pakarinen, K. Binnemans, M. Verwerft, Lattice contraction and lattice deformation of UO_2 and ThO_2 doped with Gd_2O_3, J. Nucl. Mater. 467 (Part 1) (2015) 135–143.
[2] W. Böhm, H.D. Kiehlmann, A. Nuefert, M. Peehs, Gd_2O_3 up to 9 weight percent, an established burnable poison for advanced fuel management in pressurized water reactors, Kerntechnik 1987 (50) (1987) 234.
[3] W.D. Burgos, J.T. McDonough, J.M. Senko, G. Zhang, A.C. Dohnalkova, S.D. Kelly, Y. Gorby, K.M. Kemner, Characterization of uraninite nanoparticles produced by Shewanella oneidensis MR-1, Geochim. Cosmochim. Acta 72 (20) (2008) 4901–4915.
[4] F. Cappia, R. Jovani-Abril, J. Spino, L. Luzzi, A. Janßen, D. Manara, Laser melting of nano-crystalline uranium dioxide, Prog. Nucl. Energy 72 (0) (2014) 11–16.
[5] R. Carabajal, Recent advances in magnetic sructure determination by neutron powder diffraction, Phys. B 192 (1993) 55–69.
[6] M. Durazzo, F.B.V. Oliveira, E.F. Urano de Carvalho, H.G. Riella, Phase studies in the UO_2–Gd_2O_3 system, J. Nucl. Mater. 400 (3) (2010) 183–188.
[7] S. Fukushima, T. Ohmichi, A. Maeda, H. Watanabe, The effect of gadolinium content on the thermal conductivity of near-stoichiometric $(U,Gd)O_2$ solid solutions, J. Nucl. Mater. 105 (2) (1982) 201–210.
[8] E. Hellestrand, Burnable poison reactivity control and other techniques to increase fuel burnup in LWR fuel cycles, Trans. Am. Nucl. Soc. 40 (1982) 181.
[9] S. Hu, H. Li, H. Liu, P. He, X. Wang, Nanocrystals of uranium oxide: controlled synthesis and enhanced electrochemical performance of hydrogen evolution by Ce doping, Small 11 (22) (2015) 2624–2630.
[10] S.N. Kalmykov, M.A. Denecke, Actinide Nanoparticle Research, Springer-Verlag, Berlin Heidelberg, 2011.
[11] K. Lassmann, C.T. Walker, J. van de Laar, F. Lindström, Modelling the high burnup UO_2 structure in LWR fuel, J. Nucl. Mater. 226 (1–2) (1995) 1–8.
[12] A.G. Leyva, D. Vega, V. Trimarco, D. Marchi, Homogeneity characterisation of sintered $(U,Gd)O_2$ pellets by X-ray diffraction, J. Nucl. Mater. 303 (2002) 29–33.
[13] T.M. Nenoff, S.R. Ferriera, J. Huang, D.J. Hanson, Formation of uranium based nanoparticles via gamma-irradiation, J. Nucl. Mater. 442 (1–3) (2013) 162–167.
[14] T.M. Nenoff, B.W. Jacobs, D.B. Robinson, P.P. Provencio, J. Huang, S. Ferreira, D.J. Hanson, Synthesis and low temperature in situ sintering of uranium oxide nanoparticles, Chem. Mater. 23 (23) (2011) 5185–5190.
[15] C. Pavón, Obtención y caracterización de pastillas de Uranio y Gadolinio por el método de Co-precipitación, Nuclear Engineer Instituto Balseiro Universidad de Cuyo, 2011.
[16] O. Roth, H. Hasselberg, M. Jonsson, Radiation chemical synthesis and characterization of UO_2 nanoparticles, J. Nucl. Mater. 383 (3) (2009) 231–236.
[17] T.P. Salikhov, V.V. Kan, Evaporation and condensation of uranium dioxide in an electromagnetic field, Int. J. Thermophys. 26 (4) (2005) 1215–1228.
[18] J. Spino, H. Santa Cruz, R. Jovani-Abril, R. Birtcher, C. Ferrero, Bulk-nano-crystalline oxide nuclear fuels – an innovative material option for increasing fission gas retention, plasticity and radiation-tolerance, J. Nucl. Mater. 422 (1–3) (2012) 27–44.
[19] J. Spino, K. Vennix, M. Coquerelle, Detailed characterisation of the rim microstructure in PWR fuels in the burn-up range 40–67 GWd/tM, J. Nucl. Mater. 231 (3) (1996) 179–190.
[20] P. Thompson, D.E. Cox, J.B. Hastings, Rietveld refinement of Debye-Scherrer synchrotron X-ray data from Al_2O_3, J. Appl. Crystallogr. 20 (2) (1987) 79–83.
[21] V. Tyrpekl, J.F. Vigier, D. Manara, T. Wiss, O. Dieste Blanco, J. Somers, Low

temperature decomposition of U(IV) and Th(IV) oxalates to nanograined oxide powders, J. Nucl. Mater. 460 (2015) 200–208.
[22] D.B. Williams, C.B. Carter, Transmission Electron Microscopy. A Textbook for Materials Science, Plenum Press, New York and London, 1996.
[23] B.T.M. Willis, Positions of the oxygen atoms in UO_2.13, Nature 197 (4869) (1963) 755–756.
[24] H. Wu, Y. Yang, Y.C. Cao, Synthesis of colloidal uranium-dioxide nanocrystals, J. Am. Chem. Soc. 128 (51) (2006) 16522–16523.
[25] C.E. Zvoriste-Walters, S. Heathman, R. Jovani-Abril, J.L. Spino, A. Janssen, R. Caciuffo, Crystal size effect on the compressibility of nano-crystalline uranium dioxide, J. Nucl. Mater. 435 (1–3) (2013) 123–127.
[26] S. Utsunomiya, M. Kogawa, E. Kamiishi, R.C. Ewing, Scanning Transmission Electron Microscopy and Related Techniques for Research on Actinide and RadionuclideNanomaterials. Actinide Nanoparticle Research. S. N. Kalmykov and M. A. Denecke, Springer-Verlag, Berlin Heidelberg, 2011, pp. 33–62.